Exact method for locating potential resonances and Regge trajectories

1997 J. Phys. A: Math. Gen. 30 3725

(http://iopscience.iop.org/0305-4470/30/10/041)

J. Phys. A: Math. Gen. **30** (1997) 3725–3737. Printed in the UK PII: S0305-4470(97)76759-3

Exact method for locating potential resonances and Regge trajectories

S A Sofianos and S A Rakityansky†

Physics Department, University of South Africa, PO Box 392, Pretoria 0001, South Africa

Received 25 July 1996

Abstract. We propose an exact method for locating the zeros of the Jost function for analytic potentials in the complex momentum plane. We further extend the method to the complex angular–momentum plane to provide the Regge trajectories. It is shown, by using several examples, that highly accurate results for extremely wide, as well as for extremely narrow, resonances with or without the presence of the Coulomb interaction can be obtained.

1. Introduction

Much effort has been devoted in the past to developing methods for calculating the energies and widths of resonances in the potential scattering theory. A comprehensive survey on this subject can be found in [1]. These methods can be divided into two categories. The first one is based on methods traditionally employed for real energies where one can locate the position of relatively narrow resonances with a sufficiently high accuracy, but has many difficulties in determining their widths and usually fails for broad resonances. In the second one the calculations are performed at complex energies, and therefore the widths and resonant energies are obtained simultaneously.

The complex methods have the advantage that the calculations are based on a rigorous definition of resonances, namely, as singularities of the S-matrix. Thus, in addition to the information on resonances themselves, they provide us with information about the analytic properties of the S-matrix and the off-shell properties of the underlying interaction. However, the existing complex-energy methods are much more complicated than those of the first group and require sophisticated mathematical and computational methods to handle them.

Usually, the complex methods are referred to as the 'direct calculation approaches', but very often with the quotation marks [2] because most of them are based on an expansion of the resonant wavefunction in terms of square-integrable functions and the subsequent determination of the expansion coefficients either by a diagonalization of the non-Hermitian Hamiltonian or by a variational procedure.

The method we present here formally belongs to the second group, i.e. to the complex-energy methods. It is based on exact differential equations for functions closely related to the Jost solutions and which coincide with the Jost functions at large distances [3–5]. Unlike the existing methods, it is simple to apply and although it exploits the idea of the complex rotation of the coordinates, it is different from the traditionally used complex

† Permanent address: Joint Institute for Nuclear Research, Dubna, 141980, Russia.

0305-4470/97/103725+13$19.50

dilation methods in that it does not employ expansion or variational procedures. Instead, the Jost function at a complex energy is obtained directly from exact equations equivalent to the Schrödinger equation.

To demonstrate the effectiveness and accuracy of our approach, we performed calculations using potentials previously employed by other authors [6–9]. We not only located the resonances cited by them but also found sequences of Jost function zeros corresponding to broad and extremely narrow resonances which were not considered or missed in the aforementioned references.

In addition to the location of zeros in the complex k-plane, the present method enables us to locate the zeros of Jost functions in the complex angular momentum plane. We demonstrated this by locating the zeros, known as Regge poles, representing resonances in the complex ℓ-plane.

The paper is organized as follows. In section 2 our formalism is presented, while section 3 is devoted to the boundary conditions. In section 4 the method is applied to several examples and the results obtained are discussed and compared with those obtained by other methods.

2. Basic equations

Consider the one-channel problem of two, generally charged, particles. Apart from the Coulomb force, we assume that these particles interact via a central potential $V(r)$ having the properties

$$\lim_{r\to 0} r^2 V(r) = 0 \tag{1}$$

and

$$\lim_{r\to \infty} r V(r) = 0. \tag{2}$$

The radial Schrödinger equation reads ($\hbar = 1$)

$$[\partial_r + k^2 - \ell(\ell+1)/r^2 - 2\eta k/r]\Phi_\ell(k,r) = V(r)\Phi_\ell(k,r). \tag{3}$$

The regular solutions $\Phi_\ell(k,r)$, for any complex $k \neq 0$ and complex ℓ in the half plane $\mathrm{Re}\,\ell > -\frac{1}{2}$, are defined by the boundary condition

$$\lim_{r\to 0}[\Phi_\ell(k,r)/F_\ell(\eta,kr)] = 1 \tag{4}$$

where $F_\ell(\eta,kr)$ is the regular Coulomb function [10].

In contrast to $\Phi_\ell(k,r)$, the physical solutions (bound, scattering, and Siegert states) are defined by their behaviour at large distances. However, they are all regular at $r = 0$ and thus proportional to $\Phi_\ell(k,r)$. Therefore, once the function $\Phi_\ell(k,r)$ is determined at all complex momenta k, it represents, in a most general form, all solutions of physical interest of equation (3) since any physical solution at specific values of k can be obtained from it merely by multiplying $\Phi_\ell(k,r)$ by the proper normalization constant.

At large distances $\Phi_\ell(k,r)$ can be written as a linear combination

$$\Phi_\ell(k,r) \underset{r\to\infty}{\longrightarrow} \tfrac{1}{2}[H_\ell^{(+)}(\eta,kr) f_\ell^*(\eta,k^*) + H_\ell^{(-)}(\eta,kr) f_\ell(\eta,k)]. \tag{5}$$

The functions $H_\ell^{(\pm)}(\eta,z)$ are defined in terms of the regular $F_\ell(\eta,z)$ and irregular $G_\ell(\eta,z)$ Coulomb functions [10, 11, 15],

$$H_\ell^{(\pm)}(\eta,z) \equiv F_\ell(\eta,z) \mp \mathrm{i}G_\ell(\eta,z) \tag{6}$$

and have the asymptotic behaviour,

$$H_\ell^{(\pm)}(\eta, z) \underset{|z|\to\infty}{\longrightarrow} \mp \mathrm{i} \exp\{\pm \mathrm{i}[z - \eta \ln 2z - \ell\pi/2 + \arg\Gamma(\ell + 1 + \mathrm{i}\eta)]\}. \tag{7}$$

For neutral particles or high energies where the Sommerfeld parameter $\eta \to 0$, the Coulomb functions reduce to the Riccati–Bessel, Riccati–Neumann, and Riccati–Hankel functions [10], i.e.

$$F_\ell(\eta, z) \underset{\eta\to 0}{\longrightarrow} j_\ell(z)$$
$$G_\ell(\eta, z) \underset{\eta\to 0}{\longrightarrow} -n_\ell(z)$$
$$H_\ell^{(\pm)}(\eta, z) \underset{\eta\to 0}{\longrightarrow} h_\ell^{(\pm)}(z).$$

The momentum-dependent coefficients in the above linear combination, equation (5), are the Jost functions which are analytical for all complex k of physical interest and for $\mathrm{Re}\,\ell > -\frac{1}{2}$. The last restriction on ℓ stems from the fact that at $\mathrm{Re}\,\ell = -\frac{1}{2}$ the role of $F_\ell(\eta, z)$ and $G_\ell(\eta, z)$, of being regular and irregular at the origin, is interchanged [11].

For integer (physical) ℓ the Jost function has zeros at a discrete sequence of points k_{0i}, $i = 1, 2, 3, \ldots$, situated either on the imaginary axis of the k-plane or under the real axis. At these points only the first term in the asymptotic form (5) survives, corresponding to either a bound ($\mathrm{Im}\,k > 0$) or a Siegert ($\mathrm{Im}\,k < 0$) state behaviour for large r.

On the other hand, for real values of k^2 (physical energies), the function $f_\ell(\eta, k)$ can have zeros at complex ℓ which move, with increasing k^2, along the so-called Regge trajectories which define families of bound and resonant states [11]. Therefore, when the Jost function is known at all complex values of k and at all permissible values of ℓ, it contains all the information and characteristics of the spectrum of the underlying physical system.

In [5] we proposed a method for a direct calculation of the Jost function for any complex momentum of physical interest. In this approach we use a combination of the variable constant [12] and the complex coordinate-rotation [13] methods to solve the Schrödinger equation (3) in an efficient and accurate way without resorting to any approximation, expansion, or variational (stabilization) procedures. For this, we perform a complex rotation of the coordinate r

$$r = x \exp(\mathrm{i}\theta) \qquad x \geqslant 0 \qquad \theta \in [0, \theta_{\max}] \qquad \theta_{\max} < \pi/2 \tag{8}$$

in the Schrödinger equation (3) and look for a solution in the form

$$\Phi_\ell(k, r) = \tfrac{1}{2}[H_\ell^{(+)}(\eta, kr)\mathcal{F}_\ell^{(+)}(\eta, k, x, \theta) + H_\ell^{(-)}(\eta, kr)\mathcal{F}_\ell^{(-)}(\eta, k, x, \theta)] \tag{9}$$

where $\mathcal{F}_\ell^{(\pm)}(\eta, k, x, \theta)$ are new unknown functions (variable constants) which at large x become, according to equation (5), true constants. In this way the initial value problem, defined by equations (3) and (4), reduces to the following first-order coupled differential equations

$$\partial_x \mathcal{F}_\ell^{(+)}(\eta, k, x, \theta) = \frac{\mathrm{e}^{\mathrm{i}\theta}}{2\mathrm{i}k} H_\ell^{(-)}(\eta, kr) V(r) \times [H_\ell^{(+)}(\eta, kr)\mathcal{F}_\ell^{(+)}(\eta, k, x, \theta) + H_\ell^{(-)}(\eta, kr)\mathcal{F}_\ell^{(-)}(\eta, k, x, \theta)] \tag{10}$$

$$\partial_x \mathcal{F}_\ell^{(-)}(\eta, k, x, \theta) = -\frac{\mathrm{e}^{\mathrm{i}\theta}}{2\mathrm{i}k} H_\ell^{(+)}(\eta, kr) V(r) \times [H_\ell^{(+)}(\eta, kr)\mathcal{F}_\ell^{(+)}(\eta, k, x, \theta) + H_\ell^{(-)}(\eta, kr)\mathcal{F}_\ell^{(-)}(\eta, k, x, \theta)] \tag{11}$$

with the simple boundary conditions

$$\mathcal{F}_\ell^{(+)}(\eta,k,0,\theta)=\mathcal{F}_\ell^{(-)}(\eta,k,0,\theta)=1 \tag{12}$$

which follow immediately from equations (4), (6), and (9).

In [5] it was proved that if the potential obeys conditions (1) and (2), with complex r defined by (8), then for all complex k situated above the dividing line $|k|\exp(-\mathrm{i}\theta)$ and for $x\to\infty$, the function $\mathcal{F}_\ell^{(-)}(\eta,k,x,\theta)$ has a θ-independent limit which coincides with the Jost function, i.e.

$$\lim_{x\to\infty}\mathcal{F}_\ell^{(-)}(\eta,k,x,\theta)=f_\ell(\eta,k) \tag{13}$$

while the function $\mathcal{F}_\ell^{(+)}(\eta,k,x,\theta)$ converges to $f_\ell^*(\eta,k^*)$ at all spectral points k_{0i}, $i=1,2,3,\ldots$, for which $f_\ell(\eta,k_{0i})=0$.

The proof was based on the asymptotic behaviour of the functions $H_\ell^{(\pm)}(\eta,kr)$ at large r, and can be generalized to also include the complex angular momentum ℓ. This generalization is straightforward since the angular momentum appears only in the phase factor of the asymptotic form, equation (7), and therefore for a complex ℓ the functions $\mathcal{F}_\ell^{(\pm)}(\eta,k,x,\theta)$ at large x have the same behaviour and the asymptotic relation (13) is also valid.

Thus, the procedure of calculating the Jost function is very simple since for any fixed pair of k and ℓ we only need to solve the system of first-order differential equations (10) and (11) from $x=0$ to some $x_{\max}$ where $\mathcal{F}_\ell^{(-)}(\eta,k,x,\theta)$ attains a constant value (usually, $x_{\max}$ is the range of the potential V). According to equation (13), this constant is just the Jost function $f_\ell(\eta,k)$ we are looking for. Simultaneously, as a bonus, we obtain the exact wavefunction in the form of equation (9) having the correct asymptotic behaviour. Depending on the choice of the momentum k, it can be a bound, scattering, or a Siegert state wavefunction (rotated when $\theta>0$).

The resonances in a specific region of complex k can be easily located by taking the rotation angle θ large enough to cover this region and then search for zeros of the Jost function. The zeros in the complex ℓ-plane can be similarly located with $\theta=0$.

We emphasize that this method is exact. Although we employ the complex rotation, we do not need any stabilization procedure. This has been demonstrated in [5] where we employed an analytically solvable model and showed that equations (10) and (11) give at least five-digit accuracy for the Jost function in a wide area of complex k despite the fact that the simplest Runge–Kutta method of integration was used.

3. Boundary conditions

3.1. Short distances

Formally, we have to start the integration of equations (10) and (11) from $x=0$. However, for $\ell\neq 0$ the functions $H_\ell^{(\pm)}(\eta,kr)$ are irregular, i.e. at the origin they behave as [14]

$$H_\ell^{(\pm)}(\eta,kr)\underset{r\to 0}{\longrightarrow}\frac{\mp\mathrm{i}}{2^\ell(2\ell+1)C_\ell(\eta)}\left(\frac{kr}{2}\right)^{-\ell}+\begin{cases}\mathcal{O}(\eta kr\ln kr) & \text{for } \ell=0\\ \mathcal{O}(\eta(kr)^{1-\ell}) & \text{for } \ell\neq 0\end{cases}$$

where

$$C_\ell(\eta)=\frac{2^\ell\exp(-\pi\eta/2)}{\Gamma(2\ell+2)}[\Gamma(\ell+1+\mathrm{i}\eta)\Gamma(\ell+1-\mathrm{i}\eta)]^{1/2}.$$

In [5] it was shown that the corresponding singularities at $x=0$ in the above differential equations (10) and (11) are integrable when condition (1) is fulfilled. Thus, there is no

problem from a formal point of view. However, in practical calculations we cannot start from $x = 0$ and therefore we have to shift the initial point to some small value $x_{\min}$. Thus, to implement the boundary conditions, we need to know $\mathcal{F}_\ell^{(\pm)}(\eta, k, x_{\min}, \theta)$.

There are several ways to circumvent this problem. One of them consists of transforming the differential equations, equations (10) and (11), into an equivalent pair of integral Volterra-type equations, namely,

$$\mathcal{F}_\ell^{(\pm)}(\eta, k, x, \theta) = 1 \pm \frac{\mathrm{e}^{\mathrm{i}\theta}}{\mathrm{i}k} \int_0^x H_\ell^{(\mp)}(\eta, kx'\mathrm{e}^{\mathrm{i}\theta}) V(x'\mathrm{e}^{\mathrm{i}\theta}) \Phi_\ell(k, x'\mathrm{e}^{\mathrm{i}\theta})\, \mathrm{d}x' \tag{14}$$

where $\Phi_\ell(k, r)$ is defined by equation (9). We can solve these integral equations in the interval $[0, x_{\min}]$ iteratively as follows:

$$\begin{aligned}
&\mathcal{F}_\ell^{(\pm)(0)}(\eta, k, x_{\min}, \theta) = 1 \\
&\mathcal{F}_\ell^{(\pm)(1)}(\eta, k, x_{\min}, \theta) = 1 \pm \frac{\mathrm{e}^{\mathrm{i}\theta}}{\mathrm{i}k} \int_0^{x_{\min}} H_\ell^{(\mp)}(\eta, kx\mathrm{e}^{\mathrm{i}\theta}) V(x\mathrm{e}^{\mathrm{i}\theta}) F_\ell(\eta, kx\mathrm{e}^{\mathrm{i}\theta})\, \mathrm{d}x \\
&\qquad\qquad \vdots \\
&\mathcal{F}_\ell^{(\pm)(N)}(\eta, k, x_{\min}, \theta) = 1 \pm \frac{\mathrm{e}^{\mathrm{i}\theta}}{2\mathrm{i}k} \int_0^{x_{\min}} H_\ell^{(\mp)}(\eta, kx\mathrm{e}^{\mathrm{i}\theta}) V(x\mathrm{e}^{\mathrm{i}\theta}) \\
&\qquad\qquad \times [H_\ell^{(+)}(\eta, kx\mathrm{e}^{\mathrm{i}\theta}) \mathcal{F}_\ell^{(+)(N-1)}(\eta, k, x, \theta) \\
&\qquad\qquad + H_\ell^{(-)}(\eta, kx\mathrm{e}^{\mathrm{i}\theta}) \mathcal{F}_\ell^{(-)(N-1)}(\eta, k, x, \theta)]
\end{aligned} \tag{15}$$

and then integrate the differential equations starting from the value of $\mathcal{F}_\ell^{(\pm)(N)}(\eta, k, x_{\min}, \theta)$.

For small values of $x_{\min}$ the above iteration procedure converges very fast. Moreover, when implementing the method we found that if $\mathrm{Re}\,\ell$ is small (~ 1), then a surprisingly high accuracy (better than seven digits) can be achieved even with the lowest-order iteration, equation (15). For higher values of $\mathrm{Re}\,\ell$, however, the use of these simple boundary conditions could result in numerical instabilities. This is due to the ansatz (9) which is suitable for large distances, but is not good in the vicinity of $r = 0$. Indeed, near this point the function $\Phi_\ell(k, r)$, by its definition, is regular and therefore the singularities of $H_\ell^{(+)}(\eta, kr)$ and $H_\ell^{(-)}(\eta, kr)$ are cancelled. This is secured by the boundary conditions (12). In numerical calculations, however, the cancellation of singularities is always a precarious procedure and a source of possible numerical errors. These errors increase with increasing $\mathrm{Re}\,\ell$ since in this case $H_\ell^{(\pm)}(\eta, kr)$ is more singular. Therefore, the greater $\mathrm{Re}\,\ell$ is, the further the point $x_{\min}$ must be shifted from the origin in order to avoid cancellation errors. This shift, in turn, requires more iterations of equation (14) to obtain the boundary values $\mathcal{F}_\ell^{(\pm)}(\eta, k, x_{\min}, \theta)$ to a required accuracy.

Another way to handle the boundary condition problem is to replace at short distances the ansatz (9) by a more suitable one. Indeed, this ansatz was motivated by the variable constant method [12], i.e. we looked for a solution of equation (3) in the form of a linear combination of its two independent solutions $H_\ell^{(+)}$ and $H_\ell^{(-)}$ corresponding to $V(r) \equiv 0$. When the potential is taken into account, the coefficients of this combination are r-dependent and obey equations (10) and (11). Thus, instead of $H_\ell^{(\pm)}(\eta, kr)$ we can choose another pair of linearly independent solutions, namely, $F_\ell(\eta, kr)$ and $G_\ell(\eta, kr)$, and the new ansatz reads

$$\Phi_\ell(k, r) = F_\ell(\eta, kr) A_\ell(\eta, k, x, \theta) + G_\ell(\eta, kr) B_\ell(\eta, k, x, \theta). \tag{16}$$

Since (9) and (16) are merely different representations of the same function, we have

$$\mathcal{F}_\ell^{(\pm)}(\eta, k, x, \theta) \equiv A_\ell(\eta, k, x, \theta) \pm \mathrm{i} B_\ell(\eta, k, x, \theta) \tag{17}$$

and the equations for the functions $A_\ell(\eta, k, x, \theta)$ and $B_\ell(\eta, k, x, \theta)$ are

$$\partial_x A_\ell(\eta, k, x, \theta) = \frac{e^{i\theta}}{k} G_\ell(\eta, kr) V(r)[F_\ell(\eta, kr) A_\ell(\eta, k, x, \theta) + G_\ell(\eta, kr) B_\ell(\eta, k, x, \theta)] \tag{18}$$

$$\partial_x B_\ell(\eta, k, x, \theta) = -\frac{e^{i\theta}}{k} F_\ell(\eta, kr) V(r)[F_\ell(\eta, kr) A_\ell(\eta, k, x, \theta) + G_\ell(\eta, kr) B_\ell(\eta, k, x, \theta)]. \tag{19}$$

The corresponding boundary conditions,

$$A_\ell(\eta, k, 0, \theta) = 1 \qquad B_\ell(\eta, k, 0, \theta) = 0 \tag{20}$$

follow immediately from (12) and (17).

In other words, we have two equivalent pairs of equations, equations (10), (11) and (18), (19), defining the same function $\Phi_\ell(k, r)$ in its two different representations (9) and (16). Computationally it is easier to start the integration of equations (18) and (19) at $x_{\min}$ and continue it up to some intermediate point x_{int} (not necessary small), and then to integrate equations (10) and (11) from x_{int} to $x_{\max}$ where $\mathcal{F}_\ell^{(-)}(\eta, k, x_{\max}, \theta)$ coincides with the Jost function.

Similarly to equations (10) and (11) the differential equations for $A_\ell(\eta, k, x, \theta)$ and $B_\ell(\eta, k, x, \theta)$ can be transformed into integral Volterra-type equations,

$$A_\ell(\eta, k, x, \theta) = 1 + \frac{e^{i\theta}}{k} \int_0^x G_\ell(\eta, kx' e^{i\theta}) V(x' e^{i\theta}) \Phi_\ell(k, x' e^{i\theta})\, dx' \tag{21}$$

$$B_\ell(\eta, k, x, \theta) = -\frac{e^{i\theta}}{k} \int_0^x F_\ell(\eta, kx' e^{i\theta}) V(x' e^{i\theta}) \Phi_\ell(k, x' e^{i\theta})\, dx' \tag{22}$$

where $\Phi_\ell(k, r)$ is defined by equation (16). Iterations of these integral equations can also be used to obtain corrections, if necessary, to the simplest form of the boundary conditions, namely,

$$A_\ell(\eta, k, x_{\min}, \theta) = 1 \qquad B_\ell(\eta, k, x_{\min}, \theta) = 0. \tag{23}$$

3.2. Large distances

The behaviour of $\Phi_\ell(k, r)$ at large distances, is determined by the functions $H_\ell^{(\pm)}(\eta, kr)$. Therefore, the correct asymptotic form is automatically secured.

Indeed, suppose we have found on the positive imaginary axis of the k-plane a value k_0 for which $\mathcal{F}_\ell^{(-)}(\eta, k_0, x_{\max}, 0) = 0$ (when $\operatorname{Im} k \geqslant 0$ we can always put $\theta = 0$), i.e. we located a zero of the Jost function corresponding to a bound state. The physical bound state wavefunction is then given by,

$$\varphi_\ell^{\text{bound}}(k_0, r) = \mathcal{N} \Phi_\ell(k_0, r)$$

and differs from $\Phi_\ell(k_0, r)$ only by a normalization factor $\mathcal{N}$ which can, in principle, be found along with $\Phi_\ell(k_0, r)$ in terms of the Jost function and its derivative [15, 16], or simply from the normalization integral. At large r only the first term of equation (9) survives, i.e.

$$\Phi_\ell(k_0, r) \underset{|r| \to \infty}{\longrightarrow} \tfrac{1}{2} \mathcal{F}_\ell^{(+)}(\eta, k_0, x_{\max}, 0) H_\ell^{(+)}(\eta, k_0 r). \tag{24}$$

Obviously, in this expression the exponentially decaying tail of the bound state wavefunction is presented in an exact form.

For scattering states (real positive k), the asymptotic form of $\Phi_\ell(k,r)$ contains both terms of equation (9),

$$\Phi_\ell(k,r) \underset{|r|\to\infty}{\longrightarrow} \tfrac{1}{2}[H_\ell^{(+)}(\eta,kr)\mathcal{F}_\ell^{(+)}(\eta,k,x_{\max},0) + H_\ell^{(-)}(\eta,kr)\mathcal{F}_\ell^{(-)}(\eta,k,x_{\max},0)] \tag{25}$$

where the functions $H_\ell^{(\pm)}(\eta,kr)$ represent the incoming and outgoing spherical waves (again in the exact form). The scattering wavefunction, $\varphi_{\ell,k}^{\text{scatt}}(r)$, differs from $\Phi_\ell(k,r)$ only by a constant factor, namely,

$$\varphi_{\ell,k}^{\text{scatt}}(r) = \frac{1}{2\mathcal{F}_\ell^{(-)}(\eta,k,x_{\max},0)}[H_\ell^{(+)}(\eta,kr)\mathcal{F}_\ell^{(+)}(\eta,k,x,0) + H_\ell^{(-)}(\eta,kr)\mathcal{F}_\ell^{(-)}(\eta,k,x,0)] \tag{26}$$

where we assume that the scattering states $|\Psi_{\boldsymbol{k}}^{\text{scatt}}\rangle$ are normalized according to

$$\langle\Psi_{\boldsymbol{k}'}^{\text{scatt}}|\Psi_{\boldsymbol{k}}^{\text{scatt}}\rangle = \delta(\boldsymbol{k}'-\boldsymbol{k})$$

and expand in partial waves as follows:

$$\langle\boldsymbol{r}|\Psi_{\boldsymbol{k}}^{\text{scatt}}\rangle = \sqrt{\frac{2}{\pi}}\frac{1}{kr}\sum_{\ell m} \mathrm{i}^\ell \varphi_{\ell,k}^{\text{scatt}}(r)Y_{\ell m}^*(\hat{\boldsymbol{k}})Y_{\ell m}(\hat{\boldsymbol{r}}).$$

For the Siegert states, corresponding to zeros of $\mathcal{F}_\ell^{(-)}(\eta,k,x_{\max},\theta)$ in the lower half of the k-plane, we have the same kind of asymptotic behaviour as in $\Phi_\ell(k_0,r)$ given by equation (24) but in this case $\theta > 0$, and therefore such states can be treated and normalized similarly to bound states [2].

In summary, representation (16) secures the proper behaviour of $\Phi_\ell(k,r)$ at short distances, while representation (9) guarantees its correct behaviour at large r. The use of these representations enables us to achieve high accuracy in the solution of equation (3) at all complex values of k.

4. Numerical examples

In order to demonstrate the ability and accuracy of the proposed method, we choose two simple potentials previously used in [6–9]. This choice is further motivated by the richness of the spectra generated by these potentials and by their simple form. And, as we found, their spectra include very wide, as well as extremely narrow, resonances which are difficult to locate with most of the existing methods. Thus, they are ideally suited as testing cases.

In atomic units [17], these potentials have the following form

$$V_1(r) = 7.5r^2\exp(-r) + \frac{z}{r}$$

and

$$V_2(r) = 5\exp[-0.25(r-3.5)^2] - 8\exp(-0.2r^2).$$

The reader not accustomed to the atomic units, may assume that the above potentials are given in MeV and the distances in fm. In such a case $\hbar^2/2m = \frac{1}{2}$ MeV fm^{-2} while the Sommerfeld parameter is given by $\eta = z/k$. Then the numerical values of the resonance energies are the same and independent of the unit used (MeV or atomic units). In what follows, in order to avoid possible misunderstanding, we will use the MeV fm^{-1} units. We note that $V_1(r)$ is a good case to test the ability of the method to deal with interactions having a Coulomb tail. Similarly to [9] we assumed that the Coulomb part is attractive

Table 1. The zeros k_0 of the Jost function in the complex k-plane and the energies E_0 and widths Γ of the S-wave resonances for the potential $V_1(r)$ with ($z = -1$) and without ($z = 0$) the Coulomb term.

z	k_0 (fm^{-1})	E_0 (MeV)	Γ (MeV)	Reference
0	2.617 786 172 − i0.004 879 876	3.426 390 331	0.025 548 962	this work
		3.426 39	0.025 549	[6]
		3.425 7	0.025 6	[7]
		3.426	0.025 6	[8]
		3.426	0.025 8	[9]
0	3.130 042 444 − i0.357 144 253	4.834 806 841	2.235 753 338	this work
0	3.398 392 393 − i0.997 251 873	5.277 279 780	6.778 106 356	this work
−1	1.887 074 210 − i0.000 025 362	1.780 524 536	0.000 095 719	this work
		1.780 5	0.000 095 8	[9]
−1	2.871 167 766 − i0.201 530 270	4.101 494 946	1.157 254 428	this work
−1	3.169 186 525 − i0.846 652 839	4.663 461 099	5.366 401 539	this work

with $z = -1$. In order to compare our results with those given in [6–8], we also performed calculations with $z = 0$.

To locate zeros of the Jost function in the complex k-plane as well as in the complex ℓ-plane, we searched for minima of its modulus, $|\mathcal{F}_\ell^{(-)}(\eta, k, x_{\max}, \theta)|$, considered as a function of two variables, either $\mathrm{Re}\, k$ and $\mathrm{Im}\, k$ or $\mathrm{Re}\, \ell$ and $\mathrm{Im}\, \ell$. This is based on the so-called maximum modulus principle for a complex-valued function [18]. According to this principle, when a function $f(z)$ is holomorphic and not constant in a region D of the complex plane, $|f(z)|$ can never attain its maximum in the interior of D but only on the boundary of D. Therefore the minima of $|f(z)|$ must coincide with the zeros of $f(z)$. Indeed, assuming that $|f(z)|$ has a minimum at $z = z_0$ inside the area D and $f(z_0) \neq 0$ then around the point z_0 the function $1/f(z)$ is holomorphic and has a maximum inside an area, which contradicts the maximum modulus principle. Thus, if a minimum of $|f(z)|$ is found, it must be the zero of $f(z)$.

The located zeros of the Jost function in the fourth quadrant of the complex k-plane for the potential $V_1(r)$ for the $\ell = 0$ partial wave, and the corresponding resonance energies and widths are presented in table 1 together with the results of [6–9]. Our calculations have been performed with the simplest boundary condition (23). This was sufficient to achieve an accuracy of at least nine digits. This is checked by changing the rotation angle θ since the Jost function must be θ-independent. We note that only few S-wave resonances are presented although many more were located. The reason is that this potential has already been used by several authors (but only for the case $\ell = 0$) and thus we employed it in order to compare our results with those of [6–9]. The sequence of the S-wave resonant zeros continues downwards in the complex k-plane. This behaviour can be seen in figure 1 where these zeros are plotted. A similar behaviour was also found for resonances of higher partial waves. In these cases, however, the first few zeros of the sequences are closer to the real axis (which means that they have a smaller width). The same properties were found for the resonances of the potential $V_2(r)$ which generates a richer spectrum.

A comparison with the other calculations for the potential $V_1(r)$ shows (see table 1) that only the 'direct' (dilatation) method of [6] gives an accuracy which is comparable with ours. In that reference, the five-digit accuracy was achieved by using over 40 exponentially decreasing functions in the expansion of the rotated Siegert state. In contrast, a nine-digit accuracy is achieved by our method without any exertion and, if neccessary, can easily be

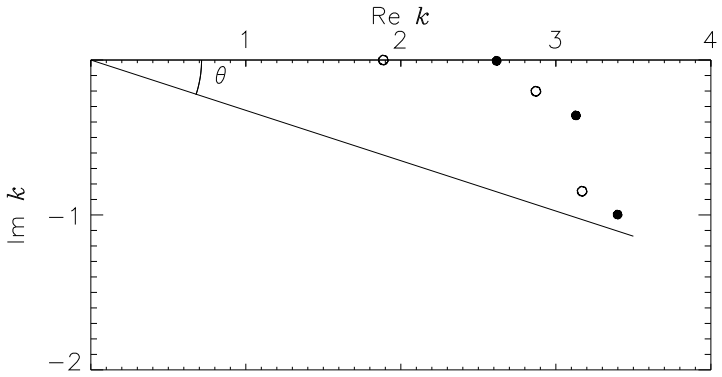

Figure 1. The zeros of the Jost function for the S-wave resonances of the potential $V_1(r)$ with (open circles) and without (full circles) the Coulomb term. Exact values are given in table 1. The dividing line corresponds to the rotation angle $\theta = 0.1\pi$.

improved. Such an improvement is of crucial importance when one deals with extremely narrow resonances. When the width of a resonance is seven orders of magnitude less than its energy, one needs at least a seven-digit accuracy to be able to discern it.

Another extreme situation is the case of very broad resonances, i.e. when the Jost function zeros are situated far below the real axis. As can be seen in table 1, even for the first resonance ($E_0 = 3.426\,390\,331$ MeV, $\Gamma = 0.025\,548\,962$ MeV) only a three-digit accuracy of the width has been achieved by the 'real-energy methods' of [7, 8] and by the 'semi-complex method' of [9] while the next, moderately broad, resonance ($E_0 = 4.834\,806\,841$ MeV, $\Gamma = 2.235\,753\,338$ MeV), is already beyond their resolution.

The 'real-energy methods' of [7, 8] consider eigenenergies of a system enclosed in a box. These eigenenergies are moving together with the change of the radius of the box, generating the so-called quasicrossings at resonance energies. The width of a resonance is determined by the width of the quasicrossing. Such an approach exploits the physical idea that the resonant states, are only slightly affected by variations of the radius of the box, in contrast to the spurious states that emerge in the box. It seems, however, that this idea is not suitable for broad resonant states. Indeed, in figure 1 of [7] and figure 1 of [8], presenting the box eigenenergies, no traces of the the second quasicrossing of the S-wave resonance at $E = 4.834\,806\,841$ MeV or of the third at $E = 5.277\,279\,780$ MeV can be found.

It is claimed that broad resonances are unimportant and thus the inability of a method to describe them is a minor drawback. However, in certain physical systems, broad resonances play a significant role. An example is the $S_{11}(1535)$ resonance of the interaction of the η-meson with a nucleon which lies 48 MeV above the threshold while its width is 150 MeV [19]. Nevertheless it prescribes the dynamics of the η-meson interaction with nuclei. In particular, due to this resonanance, certain η-nucleus systems can have quasibound states [20].

One of the advantages of the exact method presented in this work, is that bound, scattering, and resonant states can be treated in a uniform way regardless of their width. All spectral points can be located with the same accuracy irrespective of their location on the complex k-plane. This is exemplified by the spectral analysis of the potential $V_2(r)$. Sequences of the bound and resonant states generated by this potential are given in tables 2 and 3. The S- and P-wave sequences are also shown in figure 2.

The S-wave states, generated by the potential $V_2(r)$, were previously considered in [7],

Table 2. The zeros k_0 of the Jost function in the complex k-plane and the energies E_0 and widths Γ of the S-wave bound and resonant states for the potential $V_2(r)$.

ℓ	k_0 (fm^{-1})	E_0 (MeV)	Γ (MeV)	Reference
0	i3.023 634 507	−4.571 182 814	0	this work
0	i1.329 872 758	−0.884 280 776	0	this work
0	2.122 442 334 − i0.000 027 859	2.252 380 731	0.000 118 256	this work
		2.252 37	0.000 119 6	[7]
0	3.000 600 515 − i0.041 316 851	4.500 948 186	0.247 950 731	this work
		4.50	0.28	[7]
0	3.485 234 669 − i0.360 967 988	6.008 281 406	2.516 116 297	this work
0	3.974 580 284 − i0.788 297 975	7.587 937 367	6.266 307 179	this work
0	4.454 733 926 − i1.227 097 054	9.169 443 586	10.932 781 876	this work
0	4.922 800 349 − i1.664 647 328	10.731 456 273	16.389 452 891	this work
0	5.378 677 040 − i2.097 566 794	12.265 190 122	22.564 268 707	this work

Table 3. The zeros k_0 of the Jost function in the complex k-plane and the energies E_0 and widths Γ of the bound and resonant states for the potential $V_2(r)$ in several higher partial waves ($1 \leqslant \ell \leqslant 4$).

ℓ	k_0 (fm^{-1})	E_0 (MeV)	Γ (MeV)
1	i2.289 054 013	−2.619 884 138	0
1	1.270 932 606 − i0.000 000 043	0.807 634 844	0.000 000 110
1	2.674 841 953 − i0.002 433 228	3.577 386 775	0.013 017 001
1	3.263 588 553 − i0.162 882 441	5.312 239 776	1.063 162 540
1	3.742 982 846 − i0.564 324 132	6.845 729 429	4.224 511 090
1	4.225 164 261 − i0.999 000 737	8.427 005 280	8.441 884 426
1	4.696 779 393 − i1.437 816 345	9.996 210 410	13.506 212 364
1	5.156 711 217 − i1.873 567 558	11.540 707 589	19.322 893 683
2	i1.232 503 483	−0.759 532 418	0
2	2.183 644 493 − i0.000 018 973	2.384 151 637	0.000 082 862
2	3.052 966 547 − i0.035 600 651	4.659 668 666	0.217 375 191
2	3.527 492 840 − i0.341 406 094	6.163 323 809	2.408 615 103
3	1.420 585 762 − i0.000 000 016	1.009 031 953	0.000 000 046
3	2.760 769 155 − i0.001 484 354	3.810 922 062	0.008 195 917
3	3.343 986 231 − i0.139 396 664	5.581 406 240	0.932 281 051
3	3.802 701 793 − i0.526 397 919	7.091 723 079	4.003 468 620
4	2.313 665 822 − i0.000 006 013	2.676 524 768	0.000 027 824
4	3.170 315 114 − i0.023 354 979	5.025 176 235	0.148 085 287
4	3.623 738 918 − i0.294 896 551	6.522 259 887	2.137 256 217
4	4.076 486 137 − i0.706 384 524	8.059 380 065	5.759 133 441

where only the first two resonances were found. As can be seen in table 2, the spherical-box method of [7] provides the position of the first (narrow) resonance fairly well. However, the width is obtained only to two correct digits. For the second resonance, which is broader than the first one, the accuracy for the energy evaluation is down to three digits and for the width just to one digit. The other resonances of the S-wave sequence, presented in table 2, were not obtained with the box method.

The accuracy of the present method is determined by the accuracy of the solution

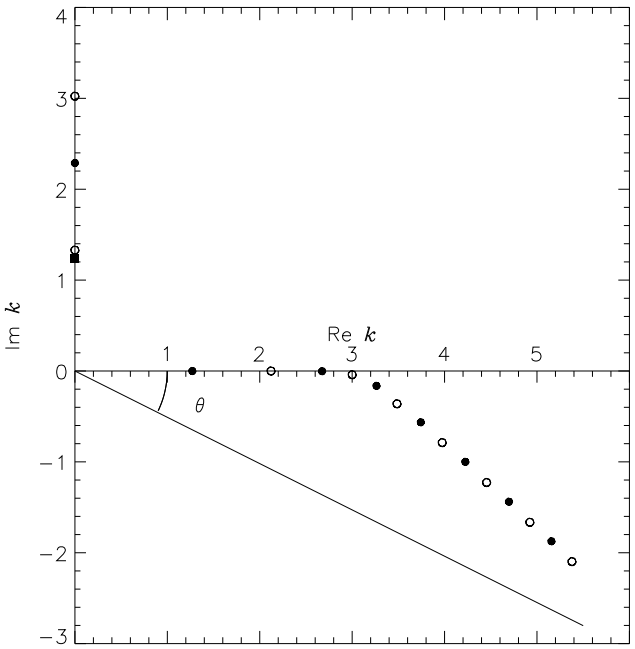

Figure 2. The zeros of the Jost function corresponding to bound and resonant states generated by the potential $V_2(r)$ in the S- (open circles) and P- (full circles) partial waves. The full box indicates the D-wave bound state. Exact values are given in tables 2 and 3. The dividing line corresponds to the rotation angle $\theta = 0.15\pi$.

Table 4. The two lowest Regge trajectories for the potential $V_2(r)$. Only those points which correspond to the bound and resonant energies are given.

First Regge trajectory		Second Regge trajectory	
E (MeV)	ℓ	E (MeV)	ℓ
−4.571 182 814	0	−0.884 280 776	0
−2.619 884 138	1	0.807 634 844	1.000 000 000 + i0.000 000 034
−0.759 532 418	2	2.384 151 637	2.000 000 000 + i0.000 027 431
1.009 031 953	3.000 000 000 + i0.000 000 013	3.810 922 062	2.999 963 480 + i0.003 081 380
2.676 524 768	4.000 000 000 + i0.000 008 632	5.025 176 235	3.990 736 977 + i0.065 066 318

of the differential equations. By choosing the tolerance to be small enough we can locate practically all resonances. Two remarkable examples of extremely narrow resonances, generated by the potential $V_2(r)$, are the one found for the P-wave at $E_0 = 0.807\,634\,844$ MeV ($\Gamma = 0.110 \times 10^{-6}$ MeV) and the other for the F-wave at $E_0 = 1.009\,031\,953$ MeV ($\Gamma = 0.46 \times 10^{-7}$ MeV) and are parts of the sequences presented in table 3. If the attraction of the potential is slightly increased, these extremely narrow resonances become bound states in the P and F partial waves.

Some of the Jost-function zeros found in the complex ℓ-plane are given in tables 4 and 5. The corresponding Regge trajectories are depicted in figure 3. Each trajectory begins from an S-wave spectral state. The first one begins from the ground state and passes via the lowest states of each partial wave. When the energy is negative, the trajectory lies on

Table 5. The third and fourth Regge trajectories for the potential $V_2(r)$. These trajectories start from the lowest S-wave resonances.

Third Regge trajectory		Fourth Regge trajectory	
E (MeV)	ℓ	E (MeV)	ℓ
2.252 380 731	$-0.000\,000\,010 + i0.000\,041\,610$	4.500 948 186	$-0.037\,200\,122 + i0.130\,360\,179$
3.577 386 775	$0.999\,888\,289 + i0.005\,370\,144$	5.312 239 776	$0.726\,629\,120 + i0.451\,038\,159$
4.659 668 666	$1.976\,641\,344 + i0.104\,936\,778$	6.163 323 809	$1.389\,037\,872 + i0.838\,973\,703$
5.581 406 240	$2.805\,402\,233 + i0.392\,410\,862$	7.091 723 079	$2.025\,517\,176 + i1.253\,031\,383$
6.522 259 887	$3.530\,415\,810 + i0.760\,317\,663$	8.059 380 065	$2.634\,772\,674 + i1.671\,995\,431$

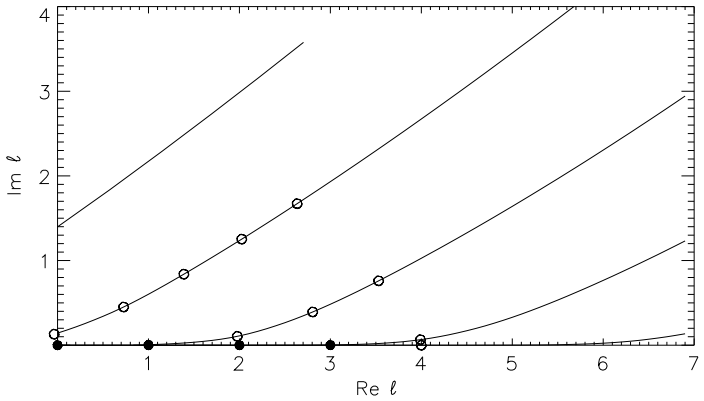

Figure 3. The five lowest Regge trajectories for the potential $V_2(r)$. Exact values of the points are given in tables 4 and 5. Full circles indicate points which coincide (they are at the same place of the ℓ-plane but correspond to different energies) or cannot be distinguished.

the real axis, while at positive energies it gradually goes upwards. We note that the width of a narrow resonance can, in principle, be found via $\mathrm{Im}\,\ell$ which corresponds to an integer value of $\mathrm{Re}\,\ell$. However, the relation between Γ and $\mathrm{Im}\,\ell$ also involves the derivative of the trajectory [16].

The Regge trajectories, can provide us with useful information on the spectrum of the physical system. They combine bound and resonant states into families and therefore in calculating such trajectories, we can find out at which energies and in which partial waves resonances must exist. Furthermore, the Regge trajectories give us a general insight into the spectrum of the Hamiltonian under consideration. For example, we can state that the F-wave resonance at $E = 1.009\,031\,953$ MeV is the narrowest one for the potential $V_2(r)$. This follows from the fact that this resonance belongs to the lowest Regge trajectory and is the first on it.

In conclusion, the method we present in this article, enables us to locate the zeros of the Jost function in the complex k-plane and to calculate the Regge trajectories in the complex ℓ-plane in a simple, efficient, and extremely accurate way. To the best of our knowledge, no other method has achieved such a performance in the past. Since it is based on exact equations, the method simultaneously provides us with the corresponding wavefunctions of the spectral states.

As a final note we mention that the method can be easily generalized to treat coupled channel problems having the same angular momentum. In such a case we replace the

potential and the functions $\mathcal{F}_\ell^{(\pm)}(\eta, k, x, \theta)$ by matrices and the spectrum is then defined by the zeros of the Jost-matrix determinant. Channels of different angular momenta can also be treated in the same manner, but this requires a more elaborate treatment of the boundary conditions at $x = 0$ since some off-diagonal elements of the matrices $\mathcal{F}_\ell^{(\pm)}$ for different ℓ may be singular at the origin. Non-local potentials can also be considered within the proposed approach. Work on all these generalizations is under way.

Acknowledgments

One of us (SAR) gratefully acknowledges financial support from the University of South Africa and the Joint Institute for Nuclear Research, Dubna, Russia.

References

[1] Kukulin V I, Krasnopolsky V M and Horaček J 1988 *Theory of Resonances* (Dortrecht: Kluwer)
[2] Rescigno T N and McCurdy C W 1986 *Phys. Rev.* A **34** 1882
[3] Pupyshev V V and Rakityansky S A 1991 *Communication of JINR (Dubna)* E4-91-418
[4] Pupyshev V V and Rakityansky S A 1994 *Z. Phys.* A **348** 227
[5] Rakityansky S A, Sofianos S A and Amos K 1996 *Nuovo Cimento* B **111** 363
[6] Isaacson A D, McCurdy C W and Miller W H 1978 *Chem. Phys.* **34** 311
[7] Maier C H, Cederbaum L S and Domcke W 1980 *J. Phys. B: At. Mol. Phys.* **13** L119
[8] Mandelshtam V A, Ravuri T R and Taylor H S 1993 *Phys. Rev. Lett.* **70** 1932
[9] Yamani H A and Abdelmonem M S 1995 *J. Phys. A: Math. Gen.* **28** 2709
[10] Abramowitz M and Stegun A (ed) 1964 *Handbook of Mathematical Functions* (Washington, DC: NBS)
[11] Taylor J R 1972 *Scattering Theory* (New York: Wiley)
[12] Mathews J and Walker R L 1964 *Mathematical Methods of Physics* (New York: Benjamin)
[13] The entire special issue of 1978 *Int. J. Quantum Chem.* **14** is devoted to the complex-coordinate method
See also the reviews: Reinhardt W P 1982 *Ann. Rev. Phys. Chem.* **33** 223
Ho Y K 1983 *Phys. Rep.* **99** 1
[14] Messiah A 1970 *Quantum Mechanics* (Amsterdam: North-Holland)
[15] Goldberger M and Watson K M 1964 *Collision Theory* (New York: Wiley)
[16] Sitenko A G 1991 *Scattering Theory* (Heidelberg: Springer)
[17] Landau L D and Lifshitz E M 1965 *Quantum Mechanics* (Oxford: Pergamon)
[18] Iyanaga S and Kawada Y (ed) 1977 *Encyclopedic Dictionary of Mathematics* (Cambridge, MA: MIT) p 159
[19] Particle Data Group 1994 *Phys. Rev.* D **50** 1319
[20] Rakityansky S A, Sofianos S A, Braun M, Belyaev V B and Sandhas W 1996 *Phys. Rev.* C **53** R2043